Strain fluctuations in $BaTiO_3/SrTiO_3$ heterostructures

V. Gartnerova[a], O. Pacherova[b], M. Klinger[a], M. Jelinek[b], A. Jager[a], M. Tyunina[b,c,]*

[a] Laboratory of Nanostructures and Nanomaterials, Institute of Physics, CAS, Na Slovance 2, 182 21 Prague, Czechia

[b]Institute of Physics, CAS, Na Slovance 2, 182 21 Prague, Czechia c Microelectronics Research Unit, Faculty of Information Technology and Electrical Engineering, University of Oulu, P.O. Box 4500, FI-90014, Finland

Epitaxy of perovskite oxide ferroelectric heterostructures with large lattice misfit is crucial for numerous emerging applications. Here we demonstrate cube-on-cube-type epitaxial growth of $BaTiO_3$ films on strongly mismatched (001)$SrTiO_3$ single-crystal substrates for the films with thicknesses significantly larger than that of misfit relaxation. The films experience strain originating from the film-substrate thermal expansion mismatch. Using a dedicated digital analysis of electron microscopy images, we show that the films contain random nanoregions of substantial strain fluctuations: the local strains vary in the range of ~(0.5–2)% compared with the average strain magnitude of ~1%. Because of strong strain-polarization coupling in ferroelectrics, fluctuations of strain produce fluctuations of polarization, which are suggested to cause relaxor-like properties in many mismatched heterostructures.

Introduction

Barium titanate ($BaTiO_3$, BTO) is an archetypical representative of perovskite-type oxide ferroelectrics [1–4]. Strong coupling between lattice strain and electrical polarization is responsible for numerous effects and unique properties of ferroelectrics enabling a variety of applications of these materials in their bulk form. Likewise, single-crystal-type epitaxial ferroelectric films are envisaged to enable numerous emerging applications. Moreover, the strain-polarization coupling makes it possible to control ferroelectric phases, phase transitions, polarization, and related response functions by varying lattice strain in epitaxial films. For heteroepitaxial films, large lattice strains can be caused by misfit between crystal symmetries, lattice parameters, and thermal expansion coefficients of the film and substrate materials. In particular, a cube-on-cube-type epitaxial ferroelectric film grown on top of a cubic substrate can experience biaxial in-plane (parallel to the substrate surface) misfit strain $s = a_s/a_f - 1$, where a_s and a_f are the lattice parameters of the substrate and unstressed film materials, correspondingly. The theoretical strain-temperature *s-T* phase diagrams of epitaxial ferroelectric films were first proposed almost two decades ago [5]. In particular, it was predicted that crystal phases, ferroelectric phases, and phase transitions in epitaxial BTO films experiencing substrate-induced strain can differ significantly from those in bulk single-crystal BTO [5,6]. Also compared with bulk, the polarization can be enhanced in the strained epitaxial films [7,8].

There is, however, a restriction to epitaxy. Indeed, elastic energy of a strained epitaxial film increases with increasing film′s thickness. When thickness reaches a critical one, the strain starts relaxing [9]. Often, the critical thickness is theoretically estimated considering complete relaxation of strain through formation of misfit dislocations [9]. The critical thickness decreases from 100 nm to (2–4) nm with increasing strain magnitude from 1% to 2.5% in perovskite oxide ferroelectric films. It means that the misfit strain can relax gradually during film growth, resulting in a distribution of strain across the thickness of the film, or in the vertical bottom-to-top direction. The residual strain is believed to monotonically decrease towards the top of the film [10]. The corresponding smooth, continuous strain gradient, which is formed additionally to the average strain, can further modify the *s-T* phase diagram and properties of ferroelectric films through flexoelectric effect [11–13].

Besides the formation of dislocations and gradual relaxation of strain, also other routes for strain relaxation exist. In particular, specific domain configurations, morphological instabilities, and defects other than dislocations assist strain relaxation [14–20]. Along with the average strain and monotonic inhomogeneous strain, also local fluctuations of lattice strain can principally exist in the films [21].

Importantly, epitaxial films for future devices should be integrated with other films and substrates, required by applications rather than determined by perfect epitaxial match. Thus, possibility for epitaxial growth of strongly mismatched ferroelectric films and knowledge of lattice strain therein are of high practical importance. Here we experimentally demonstrate epitaxy of BTO onto strongly mismatched $SrTiO_3$ (STO) substrates for BTO thickness exceeding the critical one. We also show that nanometer-size regions possessing different strains are formed in such films.

Experiment

Heteroepitaxial (50–100)-nm-thick BTO films were grown on $SrTiO_3$ (001) (STO) single-crystal substrates (MTI Corp., USA). The films were grown by pulsed laser deposition (PLD) at the substrate temperature of 973 K and oxygen pressure of 20 Pa, which was raised to 800 Pa during post deposition cooling. Compared to typical conditions for PLD of BTO, the oxygen pressure maintained here is very high, which ensures proper oxygen stoichiometry and prevents the formation of dipolar defects in BTO [22].

The crystal structure of the films was studied by x-ray diffraction (XRD) on a Bruker D8 DISCOVER SUPER SPEED SOLUTION diffractometer using Cu-Kα radiation. The Θ-2Θ scans in the range of 2Θ = 10–130 and reciprocal space maps (RSM) in the vicinity of the perovskite (002), (004), (303), (113), and (311) diffractions were measured at room-temperature. The in-plane (parallel to substrate surface) and out-of-plane (normal to substrate surface) lattice parameters were estimated from the positions of films' diffractions using EVA software and taking substrates as a reference.

The local crystal structure was inspected by transmission electron microscopy (TEM) and high-resolution transmission electron microscopy (HRTEM) using a FEI Tecnai TF20 X-twin microscope operated at 200 kV. Cross-sectional samples for the analysis were prepared by focused ion beam (FIB) milling on DualBeam scanning electron microscope FEI Quanta 3D FEG equipped with Ga+ FIB. The bright-field TEM (BF-TEM), selected area electron diffraction (SAED), and HRTEM imaging combined with fast Fourier transforms (FFT) and Fourier filtering were employed in order to investigate epitaxy, defects, and strain state in BTO.

A special procedure was applied in order to quantify spatial distribution of lattice parameters. The HRTEM images with the field of view (20 nm×20 nm) were acquired along the [100] axis of BTO. The images overlapped and covered the whole film in the out-of-plane direction. The (010) and (001) interplanar distances, corresponding to the in-plane and out-of-plane lattice parameters of BTO, were extracted from fast Fourier transforms of the images using sliding-window technique and CrysTBox diffractGUI software [23–25]. The dimensions of the windows were set to 5 nm in the out-of-plane direction and 20 nm in the in-plane direction, which ensured high accuracy with sufficient spatial resolution in the out-of-plane direction. The lattice parameters were estimated as a function of distance x from the bottom of the film using averaging and binning of the data extracted from each of the windows.

Results and discussion

The BTO-STO lattice misfit is large, 2.7% [26]. Correspondingly, the critical thickness for relaxation of misfit strain is small, a few nanometers only, in BTO on STO [17,18,27]. Despite the large misfit and small critical thickness, epitaxial growth of the BTO films with thicknesses to 100 nm is achieved on STO. Epitaxy is evidenced by XRD and TEM/HRTEM analyses. The BTO films are perovskite, highly oriented, with the (00l) planes parallel to the (001) STO substrate surface [Fig. 1].

The crystal structure of the films can be initially interpreted as pseudo-cubic. A cube-on-cube-type epitaxial growth is revealed by RSM analysis [Fig. 2]. The epitaxial relationship is [100](001)BTO || STO [100](001). Structural domains with other crystal orientations are not detected in the films.

The measured out-of-plane lattice parameter of BTO is $c_f = 0.3996$ nm, and the in-plane lattice parameters are $a_f = b_f = 0.4026$ nm. Compared with the room-temperature lattice parameters $a = b = 0.3992$ nm and c = 0.4036 nm of the tetragonal bulk BTO phase [26], the films experience anisotropic lattice strain. The in-plane strain is tensile $s_a = a_f/a - 1 = 0.9\%$, and the out-of-plane strain is compressive $s_c = c_f/c - 1 = 1\%$ in the lms. The BTO-STO lattice mismatch suggests a theoretical in-plane compressive misfit strain in BTO [26]. The detected large in-plane tensile strain implies that the expected compressive misfit strain is relaxed. The relaxation of misfit strain is consistent with the previously found critical thickness for strain relaxation being (2–4) nm only in the BTO films on STO [17,18,27]. The misfit strain is relaxed in the vicinity of the BTO-STO interface during the high-temperature growth of BTO. The room-temperature strain state results from the post-deposition cooling and corresponding build-up of thermal strain in the BTO film. The thermal strain arises from the mismatch existing between coefficients of thermal expansion in BTO and STO [26]. The room-temperature in-plane tensile thermal strain in the BTO film on STO is consistent with the theoretical model [28].

Additionally to the average (or homogeneous) strain determined from the positions of perovskite diffractions, a distribution of strain (or inhomogeneous strain) is detected by inspections of the diffractions' widths. The full width at half maximum, w, is determined for the (00l) diffractions in the Cu $K\alpha_1$ Θ-2Θ scans. The widths are analysed using the Williamson-Hall approach. The shape of diffractions is found to be best fitted by a Gaussian peak [Fig. 3(a)]. Hence, the Williamson-Hall plot of $A^2=(w\cos\Theta/\lambda)^2$ versus $(\sin\Theta/\lambda)^2$ is employed, where λ is the wavelength of the Cu $K\alpha_1$ radiation. The obtained good liner fit [Fig. 3(b)] indicates the presence of inhomogeneous strain in the film. The coherence length extracted from the linear fit is 60 nm for the 70-nm-thickfilm [Fig. 3(b)], showing that the (00l) planes of the BTO film are parallel to the substrate surface almost through the whole thickness of the film. The out-of-plane lattice parameter is distributed in the out-of-plane direction across the thickness of the film. The distribution is characterized by the relative variation ($\Delta c_f/c_f$), which is found to be approximately 0.2%. Thus, the out-of-plane compressive lattice strain possesses inhomogeneity, which can be estimated macroscopically as ~0.2%. Correspondingly, the in-plane strain is inhomogeneous, too. Next we study how inhomogeneous strains are distributed inside the films, locally.

The inhomogeneous lattice strain and details of microstructure are explored using TEM/HRTEM analyses of the BTO/STO sample. The bright-field TEM image shows the formation of vertical nanocolumns, whose lateral dimensions are (20–100) nm [Fig. 4(a)]. As previously demonstrated, such nanocolumns do not destroy epitaxy [17,20]. Also here the selected area electron diffraction pattern [Fig. 4(b)] and its simulation [Fig. 4(c)] confirm the cube-on-cube-type epitaxial growth of BTO. The columnar boundaries are randomly oriented with respect to crystal axes, that leads to contrast variation in BF/TEM and makes it difficult to assess boundaries' details. We stress that the epitaxial nanocolumns are not equivalent to grains in polycrystalline films and/or ceramics. The ceramics-type grains possess different crystal orientations, lattice strains, or phases, and may have nonstoichiometric boundaries. On contrary, the crystal structure and epitaxial relationship do not change across the boundaries between the nanocolumns. The revealed nanocolumnar microstructure of BTO is typical for strongly mismatched heteroepitaxial ferroelectric films [17–20,27].

A series of HRTEM images is acquired for (010), (011), (001), and (011) reflections. The HRTEM images show the presence of sharp STO/BTO interface. Also areas of strong contrast, indicating local strain fluctuations, are detected [Fig. 5(a)]. Despite these areas, the FFTs of the images evidence high perfection of crystal periodicity in the field of view [Fig. 5(b)].

The Fourier-filtered images reveal dislocations both in the BTO film and in the STO substrate [Fig. 5(c–f)]. The dislocations are randomly distributed. Interestingly, the Fourier-filtered images visualize regions of high contrast separated by less-contrasting regions, which points to inhomogeneity of lattice periodicity. The regions related to inhomogeneities in periodicity are large compared with the distortions around dislocations, and they are not connected with dislocations, neither with columnar boundaries. These regions are located inside the nanocolumns.

The interplanar distances are investigated inside the nanoregions, locally. For this, we apply the FFT-based approach as described in the experimental part. It is worth noting that the approach enables analysis of the periodic part in the image, which is different from the analysis of strongly confined local nonperiodicity related to separate dislocations or other defects. The approach thus allows for local quantitative analysis of crystal lattice apart from defects.

The interplanar distances are extracted from 380 sliding windows in the overlapping 38 HRTEM images acquired across the thickness of the sample. The analysis is performed at three different separate sites, randomly selected from the whole cross-sectional sample. At each site, local in-plane and out-of-plane lattice parameters of BTO are determined as a function of distance x from the bottom of the film in the vertical direction. Based on all collected data, also average lattice parameters are found. Then the strains sa and sc are calculated using the determined lattice parameters and the room-temperature lattice parameters of bulk BTO.

The results are presented in Fig. 6. A key observation is that the local strains fluctuate around the average values in BTO. Fluctuations of lattice parameters are not detected in the STO substrate. Note that the average strain values determined by HRTEM in BTO are in a good agreement with the XRD results. The local fluctuations of strain are substantial: the local strains vary in the range of approximately (0.5–2)% compared with the average strain magnitude of ~1%. Importantly, the strain fluctuations are randomly distributed in space. Thus the inhomogeneous strain is not a monotonic function of coordinate.

The dimensions of regions possessing uniform strains or uniform strain gradients are of several to tens of nanometers. We emphasize that the detected nanoregions are not directly connected to dislocations or boundaries between the columns. The nanoregions can be caused by non-uniform long-range stress fields, which result from the film-substrate elastic coupling and also from such structural irregularities as dislocations and boundaries.

Because of strong strain-polarization coupling in BTO, fluctuations of lattice strain can produce significant fluctuations of polarization [5–8]. Correspondingly, the BTO film, containing random nanoregions of different lattice strains, can be thought as containing nanoregions of different local polarizations. As known, polar nanoregions are responsible for many unique properties of ferroelectric relaxors [3,4,29–32]. The relaxor polar nanoregions are related to chemical inhomogeneity on the scale of a few nanometers. Considering relaxors, a chemical inhomogeneity has been proposed to explain unusual relaxor-like features also in epitaxial films of normal ferroelectrics or paraelectrics [33–36]. Our experimental observations imply that strain inhomogeneity can create polar nanoregions, leading to relaxor-like behaviour in epitaxial films of ferroelectrics [33–38], including the studied BTO films on STO [39]. We emphasize that strain-induced polar nanoregions differ from those in relaxors because of the presence of ferroelectricity, strong long-range elastic interactions, and larger [16] dimensions of the regions in epitaxial films. Nevertheless, such important relaxor-like properties as high dielectric constants and large dynamic nonlinearity can be produced by polar nanoregions [17] originating from strain fluctuations.

Conclusions

Cube-on-cube-typeepitaxialgrowthofperovskiteoxide ferroelectric $BaTiO_3$ films is achieved on strongly mismatched (001)$SrTiO_3$ single-crystal substrates. Epitaxy is demonstrated in the films with thicknesses significantly exceeding the critical [20] thickness for relaxation of the large film-substrate misfit strain. The in-plane compressive misfit strain is relaxed during the high-temperature growth. The tensile in-plane strain is built up during cooling because of the film-substrate thermal expansion mismatch. The films contain random nanoregions of substantial strain fluctuations. Because of strong strain-polarization coupling in ferroelectrics, the local fluctuations of strain are suggested to cause polarization fluctuations, responsible for relaxor-like properties in many mismatched heterostructures.

Acknowledgement

The work was supported by the Grant Agency of the Czech Republic (Grant No. 15-15123S).

References

[1] M.E. Lines, A.M. Glass, Principles and Applications of Ferroelectrics and Related Materials, Clarendon Press, Oxford, 2004.

[2] B.A. Strukov, A.P. Levanyuk, Ferroelectric Phenomena in Crystals: Physical Foundations, Springer-Verlag, Berlin Heidelberg, 1998.

[3] G.A. Smolenskii, V.A. Bokov, V.A. Isupov, N.N. Krainik, R.E. Pasynkov, A.I. Sokolov, Ferroelectrics and Related Materials, Gordon Breach, New York, 1984.

[4] R. Blinc, Advanced Ferroelectricity, Oxford University Press, Oxford, 2011.

[5] N.A. Pertsev, A.G. Zembilgotov, A.K. Tagantsev, Effect of mechanical boundary conditions on phase diagrams of epitaxial ferroelectric thin films, Phys. Rev. Lett. 80 (1998) 1988.

[6] O. Diéguez, K.M. Rabe, D. Vanderbilt, First-principles study of epitaxial strain in perovskites, Phys. Rev. B 72 (2005) 144101.

[7] C. Ederer, N.A. Spaldin, Effect of epitaxial strain on the spontaneous polarization of thin film ferroelectrics, Phys. Rev. Lett. 95 (2005) 257601.

[8] N.A. Pertsev, B. Dkhil, Strain sensitivity of polarization in perovskite ferroelectrics, Appl. Phys. Lett. 93 (2008) 122903.

[9] M. Ohring, Materials Science of Thin Films, Academic Press, San Diego, 2001.

[10] G. Catalan, B. Noheda, J. McAneney, L.J. Sinnamon, J.M. Gregg, Strain gradients in epitaxial ferroelectrics, Phys. Rev. B 72 (2005) 020102(R).

[11] P. Zubko, G. Catalan, A.K. Tagantsev, Flexoelectric effect in solids, Annu. Rev. Mater. Res. 43 (2013) 387.

[12] D. Lee, A. Yoon, S.Y. Jang, J.G. Yoon, J.S. Chung, M. Kim, J.F. Scott, T.W. Noh, Giant flexoelectric effect in ferroelectric epitaxial thin films, Phys. Rev. Lett. 107 (2011) 057602.

[13] A. Kvasov, A.K. Tagantsev, Dynamic flexoelectric effect in perovskites from first-principles calculations, Phys. Rev. B 92 (2015) 054104.

[14] J.S. Speck, W. Pompe, Domain configurations due to multiple misfit relaxation mechanisms in epitaxial ferroelectric thin films: I. Theory, J. Appl. Phys. 76 (1994) 466.

[15] J.S. Speck, A. Seifert, W. Pompe, R. Ramesh, Domain configurations due to multiple misfit relaxation mechanisms in epitaxial ferroelectric thin films. II. Experimental verification and implications, J. Appl. Phys. 76 (1994) 477.

[16] J.S. Speck, A.C. Daykin, A. Seifert, A.E. Romanov, W. Pompe, Domain configurations due to multiple misfit relaxation mechanisms in epitaxial ferroelectric thin films. III. Interfacial defects and domain misorientations, J. Appl. Phys. 78 (1995) 1696.

[17] J.Q. He, E. Vasco, R. Dittmann, R.H. Wang, Growth dynamics and strain relaxation mechanisms in $BaTiO_3$ pulsed laser deposited on $SrRuO_3/SrTiO_3$, Phys. Rev. B 73 (2006) 125413.

[18] A. Visinoiu, M. Alexe, H.N. Lee, D.N. Zakharov, A. Pignolet, D. Hesse, U. Gösele, Initial growth stages of epitaxial $BaTiO_3$ films on vicinal $SrTiO_3$(001) substrate surfaces, J. Appl. Phys. 91 (2002) 10157.

[19] X.W. Wang, X. Wang, W.J. Gong, Y.Q. Zhang, Y.L. Zhu, Z.J. Wang, Z.D. Zhang, Microstructure and ferroelectric properties of epitaxial BaTiO3/$SrRuO_3$/ $SrTiO_3$(001) films grown by pulsed laser deposition under high oxygen pressure, Thin Solid Films 520 (2012) 2785.
[20] M. Tyunina, L. Yao, M. Plekh, J. Levoska, S. van Dijken, Epitaxial ferroelectric heterostructures with nanocolumn-enhanced dynamic properties, Adv. Funct. Mater. 23 (2013) 467.
[21] M.W. Chu, I. Szafraniak, R. Scholz, C. Harnagea, D. Hesse, M. Alexe, U. Gösele, Impact of misfit dislocations on the polarization instability of epitaxial nanostructured ferroelectric perovskites, Nat. Mater. 3 (2004) 87.
[22] A. R. Damodaran, E. Breckenfeld, Z. Chen, S. Lee, L.W. Martin, Enhancement of ferroelectric curie temperature in $BaTiO_3$ films via strain-induced defect dipole alignment, Adv. Mater. 26 (2014) 6341.
[23] M. Klinger, M. N _emec, L. Polívka, V. Gärtnerová, A. Jäger, Automated CBED processing: sample thickness estimation based on analysis of zone-axis CBED pattern, Ultramicroscopy 150 (2015) 88.
[24] M. Klinger, A. Jäger, Crystallographic Tool Box (CrysTBox): automated tools for transmission electron microscopists and crystallographers, J. Appl. Cryst. 48 (2015) 2012.
[25] M. Klinger, L. Polıvka, A. Jager, M. Tyunina, Quantitative analysis of structural inhomogeneity in nanomaterials using transmission electron microscopy, J. Appl. Cryst. 49 (2016) 762.
[26] K.H. Hellwege, A.M. Hellwege (Eds.), Landolt-Börnstein. Numerical Data and Functional Relationships in Science and Technology. New Series. Group III. Crystal and Solid State Physics, Springer, Berlin, 1981.
[27] H.P. Sun, W. Tian, X.Q. Pan, J.H. Haeni, D.G. Schlom, Evolution of dislocation arrays in epitaxial BaTiO3 thin films grown on (100) SrTiO3, Appl. Phys. Lett. 84 (2004) 3298.
[28] V.B. Shirokov, Y.I. Yuzyuk, B. Dkhil, V.V. Lemanov, Phenomenological theory of phase transitions in epitaxial BaTiO3 thin films, Phys. Rev. B 75 (2007) 224116.
[29] G.A. Smolenskii, V.A. Isupov, A.I. Agranovskaya, S.N. Popov, Ferroelectrics with diffuse phase transitions, Sov. Phys. Solid State 2 (1961) 2584.
[30] L.E. Cross, Relaxor ferroelectrics: an overview, Ferroelectrics 151 (1994) 305.

[31] A.A. Bokov, Z.G. Ye, Recent progress in relaxor ferroelectrics with perovskite structure, J. Mater. Sci. 41 (2006) 31.

[32] V.V. Shvartsman, D.C. Lupascu, Lead-free relaxor ferroelectrics, J. Am. Ceram. Soc. 95 (2012) 1.

[33] D.A. Tenne, A. Soukiassian, M.H. Zhu, A.M. Clark, X.X. Xi, H. Choosuwan, Q. He, R. Guo, A.S. Bhalla, Raman study of BaxSr1-xTiO3 films: evidence for the existence of polar nanoregions, Phys. Rev. B 67 (2003) 012302.

[34] M. Tyunina, J. Levoska, Coexistence of ferroelectric and relaxor properties in epitaxial films of Ba_xSr_{1-x} TiO_3, Phys. Rev. B 70 (2004) 132105.

[35] M.D. Biegalski, Y. Jia, D.G. Schlom, S. Trolier-McKinstry, S.K. Streiffer, V. Sherman, R. Uecker, P. Reiche, Relaxor ferroelectricity in strained epitaxial $SrTiO_3$ thin films on $DyScO_3$ substrates, Appl. Phys. Lett. 88 (2006) 192907.

[36] H.W. Jang, A. Kumar, S. Denev, M.D. Biegalski, P. Maksymovych, C.W. Bark, C.T. Nelson, C.M. Folkman, S.H. Baek, N. Balke, C.M. Brooks, D.A. Tenne, D.G. Schlom, L.Q. Chen, X.Q. Pan, S.V. Kalinin, V. Gopalan, C.B. Eom, Ferroelectricity in strain-free $SrTiO_3$ thin films, Phys. Rev. Lett. 104 (2010) 197601.

[37] M. Tyunina, J. Levoska, I. Jaakola, Dynamic disorder in $BaTiO_3$ epitaxial films, Phys. Rev. B 75 (2007) 140102(R).

[38] R. Wördenweber, J. Schwarzkopf, E. Hollmann, A. Duk, B. Cai, M. Schmidbauer, Impact of compressive in-plane strain on the ferroelectric properties of epitaxial $NaNbO_3$ films on (110) $NdGaO_3$, Appl. Phys. Lett. 103 (2013) 132908.

[39] M. Tyunina, M. Savinov, Dynamic nonlinearity in epitaxial BaTiO3 films, Phys. Rev. B 94 (2016) 054109.

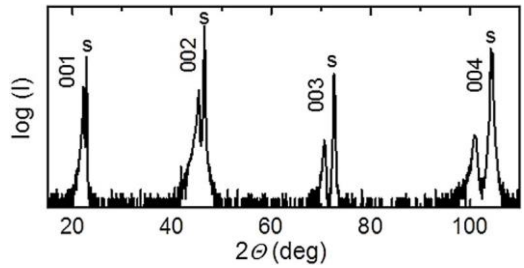

Fig. 1. X-ray diffraction Θ-2Θ scan. Substrate diffractions are marked by s.

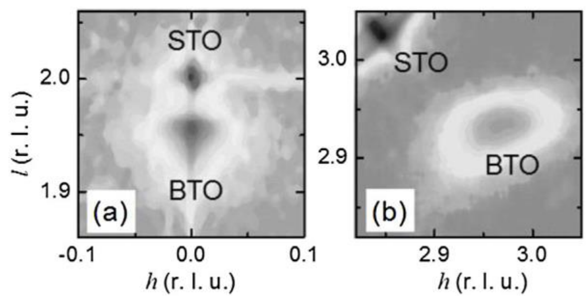

Fig. 2. Reciprocal space maps (a) for (002) and (b) for (303) directions. The results are presented in reciprocal lattice units (r.l.u.) of STO.

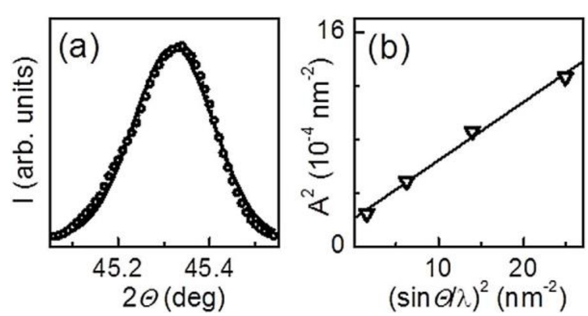

Fig. 3. (a) X-ray diffraction Θ-2Θ scan around perovskite BTO (002) peak in the 70-nm-thick BTO film on STO. Solid curve shows the Gaussian fit. (b) The Williamson-Hall plot for the (00l) diffractions. Straight line shows the fit.

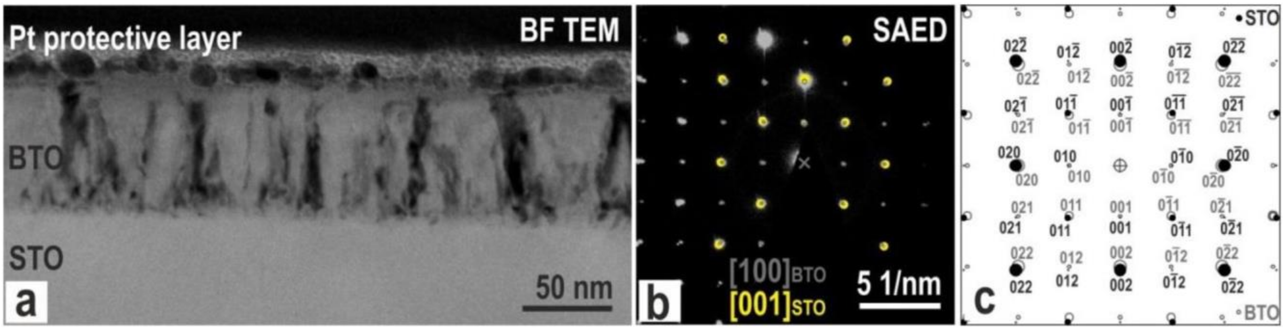

Fig. 4. TEM analysis of the BTO/STO cross-section. (a) BF TEM image. (b) SAED pattern in the [100] BTO direction. (c) Simulated diffraction patterns in the [001] STO and [100] BTO directions.

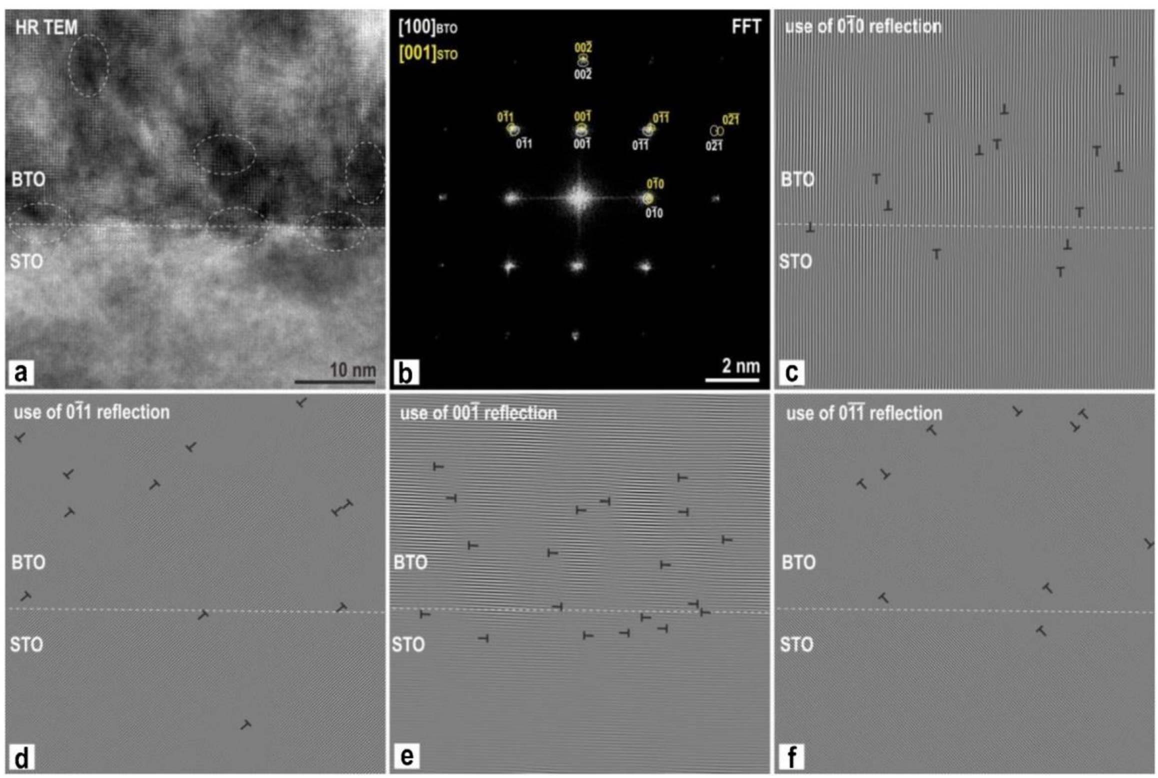

Fig. 5. HRTEM analysis of the BTO/STO cross-section. (a) HRTEM image. The STO/BTO interface is shown by the straight dashed line. Also areas of strong contrast (indicating local strain) are marked. (b) FFT of the image in (a). (c–f) Fourier-filtered images. The reflections and dislocations are marked in the images. The STO/BTO interface is shown by the straight dashed line.

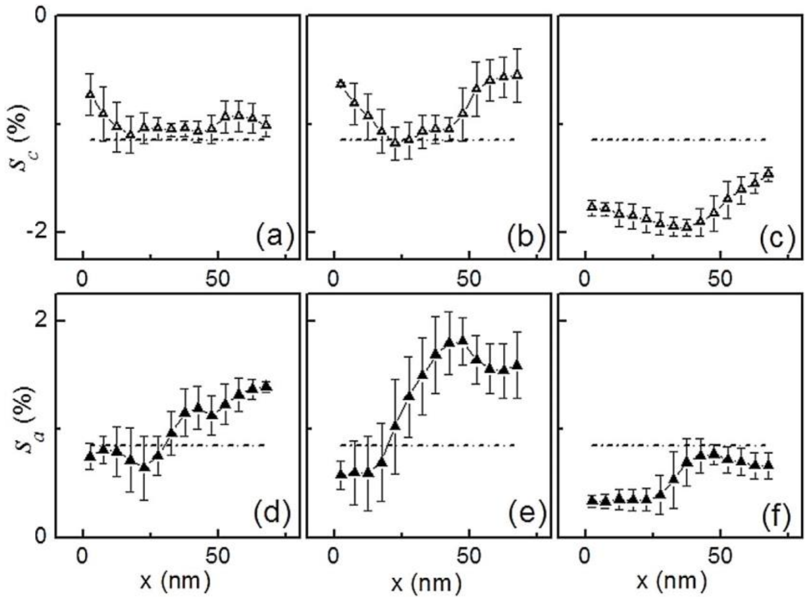

Fig. 6. (a–c) The out-of-plane strain s_c and (d–f) in-plane strain s_a determined by HRTEM/FFT analysis at three separate sites of the sample: site I (a,d), site II (b,e), and site III f). The average strains are shown by dashed lines.